Transp Porous Med
DOI 10.1007/s11242-013-0198-y

Convective Instability in a Horizontal Porous Channel with Permeable and Conducting Side Boundaries

Antonio Barletta · Eugenia Rossi di Schio · Leiv Storesletten

Received: 30 May 2013 / Accepted: 11 June 2013

Abstract The stability analysis of the motionless state of a horizontal porous channel with rectangular cross-section and saturated by a fluid is developed. The heating from below is modelled by a uniform flux, while the top wall is assumed to be isothermal. The side boundaries are considered as permeable and perfectly conducting. The linear stability of the basic state is studied for the normal mode perturbations. The principle of exchange of stabilities is proved, so that only stationary normal modes need to be considered in the stability analysis. The eigenvalue problem for the neutral stability condition is solved analytically, and a closed-form dispersion relation is obtained for the neutral stability. The Darcy–Rayleigh number is expressed as an implicit function of the longitudinal wave number and of the aspect ratio. The critical wave number and the critical Darcy–Rayleigh number are evaluated for different aspect ratios. The preferred modes under critical conditions are detected. It is found that the selected patterns of instability at the critical Rayleigh number are two-dimensional, for slender or square cross-sections of the channel. On the other hand, instability is three dimensional when the critical width-to-height ratio, 1.350517, is exceeded. Eventually, the effects of a finite longitudinal length of the channel are discussed.

Keywords Porous medium · Linear stability · Rectangular channel · Darcy–Bénard problem · Uniform heat flux

A. Barletta (✉)· E. Rossi di Schio
Department of Industrial Engineering, Alma Mater Studiorum Università di Bologna,
Viale Risorgimento 2, 40136 Bologna, Italy
e-mail: antonio.barletta@unibo.it

E. Rossi di Schio
e-mail: eugenia.rossidischio@unibo.it

L. Storesletten
Department of Mathematics, University of Agder, Postboks 422, 4604 Kristiansand, Norway
e-mail: leiv.storesletten@uia.no

Published online: 25 June 2013

1 Introduction

In the last decades, many authors have investigated the onset of convection in a fluid saturated porous medium heated from below, starting from the pioneering papers by Horton and Rogers (1945), and by Lapwood (1948). Nowadays, this topic is termed, in a wide sense, either Horton–Rogers–Lapwood problem, or Darcy–Bénard problem. Surveys on the main results obtained in this field were written by Rees (2000), Tyvand (2002), Nield and Bejan (2006), Straughan (2008), Barletta (2011). The Darcy–Bénard problem was originally formulated for an infinitely wide horizontal saturated porous layer in a motionless state, bounded by two horizontal, isothermal, and impermeable walls maintained at different temperatures. In later investigations, various types of thermal boundary conditions, involving all possible combinations of isothermal and isoflux conditions, were analysed. Furthermore, the condition of a finite lateral width of the channel was analysed as well. The case of a horizontal porous channel with rectangular cross-section was studied by Sutton (1970), Beck (1972), and further explored by Nilsen and Storesletten (1990).

Recently, Barletta and Storesletten (2012) have studied the onset of convection in a horizontal rectangular channel, bounded above and below with impermeable isothermal walls at different temperatures, but with external convection conditions through the sidewalls. These authors carried out a three-dimensional linear stability analysis both for a channel with a longitudinal infinite length and for a finite longitudinal length. The linear disturbance equations were solved by Galerkin's method of weighted residuals, as well as by a sixth-order Runge–Kutta method combined with the shooting method. The thermal behaviour of the vertical sidewalls was modelled through a Biot number associated with the convection to an external, thermally stratified, fluid environment.

The aim of the present paper is to further develop the analysis presented in Barletta and Storesletten (2012). We will consider a horizontal rectangular porous channel, having infinite length in the longitudinal direction. The lower horizontal wall is impermeable and subject to an upward uniform heat flux, while the upper horizontal wall is impermeable and isothermal. The side boundaries are assumed to be permeable as well as in perfect thermal and mechanical contact with an external porous reservoir. The reservoir is saturated by the same fluid and thermally stratified in the vertical direction, so that Dirichlet temperature and pressure conditions can be prescribed. The local momentum balance is modelled by Darcy's law, while the local energy balance is formulated by assuming local thermal equilibrium between the solid and the fluid phase. With the fluid that saturates the porous channel initially at rest, a three-dimensional linear stability analysis will be carried out. The governing equations for the linear disturbances of the basic state will be solved analytically. The neutral stability curves, as well as the critical values of the Darcy–Rayleigh number, will be determined for assigned values of the transverse aspect ratio. Finally, the effects of a finite longitudinal length will be studied, thus discussing the modes selection at the onset of the instability. In this regard, different assumptions will be made about the velocity and pressure conditions at the end boundaries in the longitudinal direction.

2 Problem Statement

Thermal convection in a porous material saturated by a fluid is considered. Let the porous medium occupy a channel with rectangular cross-section, bounded by two horizontal impermeable walls, at $\bar{y} = 0$ and $\bar{y} = H$, and laterally confined at $\bar{x} = 0$ and $\bar{x} = L$ (see Fig. 1).

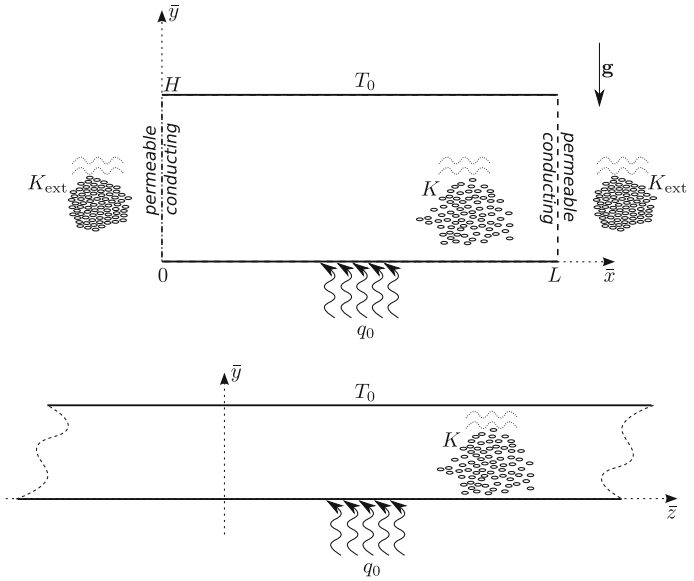

Fig. 1 Sketch of the rectangular porous channel

Gravity acts in the negative y-direction, so that $\mathbf{g} = -g\,\mathbf{e}_y$ is the gravitational acceleration, with modulus g and $\mathbf{e}_y$ is the unit vector along the vertical $\bar{y}$ axis.

2.1 Mathematical Model

In the following, the dimensional fields, coordinates, time, and nabla operator are denoted by an over-line. The components of the seepage velocity $\bar{\mathbf{u}}$, relative to the Cartesian set of coordinates $(\bar{x}, \bar{y}, \bar{z})$, are denoted as $(\bar{u}, \bar{v}, \bar{w})$, respectively.

Let us assume that:

- the porous medium is homogeneous and isotropic;
- the solid and fluid phases are in local thermal equilibrium;
- Darcy's law and the Oberbeck–Boussinesq approximation are satisfied;
- the effect of viscous dissipation is negligible.

The local balance equations of mass, momentum, and energy can be written as

$$\bar{\boldsymbol{\nabla}} \cdot \bar{\mathbf{u}} = 0, \tag{1a}$$

$$\frac{\mu}{K}\,\bar{\mathbf{u}} = -\bar{\boldsymbol{\nabla}}\,\bar{p} + \rho\, g\, \beta\, \left(\bar{T} - T_0\right) \mathbf{e}_{\mathrm{y}}, \tag{1b}$$

$$\sigma\,\frac{\partial \bar{T}}{\partial \bar{t}} + \bar{\mathbf{u}} \cdot \bar{\boldsymbol{\nabla}}\bar{T} = \alpha\,\bar{\nabla}^2\bar{T}, \tag{1c}$$

where μ is the dynamic viscosity, K is the permeability, $\bar{p}$ is the dynamic pressure, viz. the local difference between the pressure and the hydrostatic pressure, ρ is the reference density, β is the thermal expansion coefficient, $\bar{t}$ is the time, $\bar{T}$ is the temperature and T_0 is the reference temperature, α is the average thermal diffusivity, σ is the ratio between the average volumetric heat capacity of the fluid-saturated porous medium and the volumetric heat capacity of the fluid.

2.2 Boundary Conditions

The lower horizontal wall ($\bar{y} = 0$) is subject to a positive uniform heat flux $q_0 = k\,\Delta T/H$, with k denoting the average thermal conductivity of the saturated porous medium, and ΔT being a reference temperature difference. On the other hand, the upper wall ($\bar{y} = H$) is isothermal with temperature T_0. The lateral boundaries ($\bar{x} = 0, L$) are assumed to be perfectly permeable and in perfect thermal contact with an external porous reservoir saturated by the same fluid. The external reservoir is in a steady state. The vertical distributions of temperature and pressure in the external reservoir, close to the boundaries $\bar{x} = 0$ and $\bar{x} = L$, are given by

$$\bar{T}_{\rm ext}(\bar{y}) = T_0 + \Delta T\left(1 - \frac{\bar{y}}{H}\right), \qquad \bar{p}_{\rm ext}(\bar{y}) = p_0 + \rho g\beta\Delta T\,\bar{y}\left(1 - \frac{\bar{y}}{2H}\right), \tag{2}$$

where p_0 is a constant reference pressure. The permeability $K_{\rm ext}$ of the porous reservoir external to the rectangular channel is assumed to be much smaller than K, so that the steady state in the reservoir remains stable in spite of the possible onset of convection instability inside the porous channel. We will further comment on this assumption in Sect. 2.5. It is worth mentioning that models of partially permeable and partially conducting thin porous sidewalls were recently formulated and employed for analyses of thermal stability in porous media by Nygård and Tyvand (2010, 2011).

On account of Eq. (2), the boundary conditions can be expressed as follows:

$$\begin{aligned}
&\bar{y} = 0; \quad 0 < \bar{x} < L: && \bar{v} = 0, \quad -k\,\frac{\partial\bar{T}}{\partial\bar{y}} = q_0,\\
&\bar{y} = H; \quad 0 < \bar{x} < L: && \bar{v} = 0, \quad \bar{T} = T_0,\\
&\bar{x} = 0, L; \quad 0 < \bar{y} < H: && \bar{p} = \bar{p}_{\rm ext}(\bar{y}), \quad \bar{T} = \bar{T}_{\rm ext}(\bar{y}).
\end{aligned} \tag{3}$$

2.3 Dimensionless Formulation

Dimensionless quantities are defined such that

$$(\bar{x}, \bar{y}, \bar{z}) = (x,\ y,\ z)\,H, \quad \bar{\mathbf{u}} = (\bar{u}, \bar{v}, \bar{w}) = (u,\ v,\ w)\,\frac{\alpha}{H} = \mathbf{u}\,\frac{\alpha}{H},$$

$$\bar{\boldsymbol{\nabla}} = \frac{1}{H}\boldsymbol{\nabla}, \quad \bar{T} = T_0 + \frac{q_0 H}{k}\,T, \quad \bar{p} = p_0 + \frac{\mu\,\alpha}{K}\,p, \quad \bar{t} = \frac{\sigma\,H^2}{\alpha}\,t, \quad s = \frac{L}{H}. \tag{4}$$

The governing equations (1) can thus be rewritten in a dimensionless form as

$$\boldsymbol{\nabla}\cdot\mathbf{u} = 0, \tag{5a}$$

$$\mathbf{u} = -\boldsymbol{\nabla}p + R\,T\,\mathbf{e}_y, \tag{5b}$$

$$\frac{\partial T}{\partial t} + \mathbf{u}\cdot\boldsymbol{\nabla}T = \nabla^2 T. \tag{5c}$$

Here, R is the Darcy–Rayleigh number given by

$$R = \frac{\rho g\beta\Delta T\,K\,H}{\mu\alpha}. \tag{6}$$

The boundary conditions defined by Eqs. (2) and (3) can be rewritten as

$$\begin{aligned}
&y = 0; \quad 0 < x < s: && v = 0, \quad \frac{\partial T}{\partial y} = -1,\\
&y = 1; \quad 0 < x < s: && v = 0, \quad T = 0,\\
&x = 0, s; \quad 0 < y < 1: && p = R\,y\left(1 - \frac{y}{2}\right), \quad T = 1 - y.
\end{aligned} \tag{7}$$

2.4 Basic Solution

A stationary solution of Eqs. (5) and (7) is given by

$$u_\mathrm{b} = v_\mathrm{b} = w_\mathrm{b} = 0, \qquad T_\mathrm{b} = 1 - y, \qquad p_\mathrm{b} = R\, y \left(1 - \frac{y}{2}\right), \tag{8}$$

where subscript "b" means "basic solution". Equation (8) defines a rest state of the saturating fluid with a uniform vertical temperature gradient.

2.5 Permeable Sidewalls

The thermoconvective instability is governed by the value of R. Its onset is determined by a sufficiently large R. Equation (6) suggests that the same reference temperature difference, ΔT, may produce a higher value of R in the porous channel, where the permeability is K, and a significantly lower value in the external porous medium (the domain $x < 0$ and $x > s$), where the permeability, K_ext, is considerably lower than K. When R becomes critical, viz. sufficiently large for the onset of instability in the porous channel, the Darcy–Rayleigh number in the external porous medium is still subcritical. Thus, the same ΔT may be sufficient for the onset of instability inside the channel, but insufficient in the external medium.

This reasoning justifies our model of an external medium constraining the vertical pressure distribution at the sidewalls, while the onset of convection cells is observed inside the channel. This model is applicable as long as we are dealing with a basic rest state, Eq. (8), and with a linear stability analysis of this basic state. In fact, the forthcoming analysis will be based on the assumption of small-amplitude perturbations of the pressure and temperature fields. Our task is just to detect in what circumstances convection initiates. On the other hand, the behaviour when convection is well established (nonlinear, or supercritical regime), that is when the velocity components have finite or large values, is beyond our present goals. We just mention that, in the nonlinear regime, the interaction at the sidewalls between the internal porous medium and the external porous medium, and hence the formulation of the boundary conditions at $x = 0$ and $x = s$, are possibly affected by the finite flow rates associated with the internal convection cells.

3 Linear Stability Analysis

A pressure–temperature formulation of Eqs. (5) is now adopted, by substituting Eq. (5b) into Eqs. (5a) and (5c). Thus, we obtain

$$\nabla^2 p = R\, \frac{\partial T}{\partial y}, \tag{9a}$$

$$\nabla^2 T = \frac{\partial T}{\partial t} - \nabla p \cdot \nabla T + R\, T\, \frac{\partial T}{\partial y}. \tag{9b}$$

The boundary conditions, Eq. (7), can be rewritten as

$$\begin{aligned}
&y = 0; \quad 0 < x < s: && \frac{\partial p}{\partial y} = R\, T, \quad \frac{\partial T}{\partial y} = -1,\\
&y = 1; \quad 0 < x < s: && \frac{\partial p}{\partial y} = 0, \quad T = 0,\\
&x = 0, s; \quad 0 < y < 1: && p = R\, y \left(1 - \frac{y}{2}\right), \quad T = 1 - y.
\end{aligned} \tag{10}$$

We disturb the basic solution, Eq. (8), with small-amplitude perturbations, namely

$$p = p_b + \varepsilon\, P, \qquad T = T_b + \varepsilon\, \theta. \tag{11}$$

Following the usual linear stability analysis, we substitute Eq. (11) into Eqs. (9) and we neglect the terms of order ε^2. As a consequence, Eqs. (9) yield

$$\nabla^2 P = R\,\frac{\partial \theta}{\partial y}, \tag{12a}$$

$$\nabla^2 \theta = \frac{\partial \theta}{\partial t} - R\,\theta + \frac{\partial P}{\partial y}, \tag{12b}$$

while Eq. (10) leads to the boundary conditions

$$\begin{aligned} &y = 0; \quad 0 < x < s: && \frac{\partial P}{\partial y} = R\,\theta, \quad \frac{\partial \theta}{\partial y} = 0, \\ &y = 1; \quad 0 < x < s: && \frac{\partial P}{\partial y} = 0, \quad \theta = 0, \\ &x = 0, s; \quad 0 < y < 1: && P = 0, \quad \theta = 0. \end{aligned} \tag{13}$$

We imposed the continuity of pressure and temperature across the vertical sidewalls, $x = 0$ and $x = s$. Thus, the dimensionless boundary conditions for the disturbances are $P = 0$ and $\theta = 0$. We mention that, on modelling a vertical permeable interface between a porous medium and a reservoir, Rees and Tyvand (2004) assume that the velocity component parallel to the interface is zero, so that one obtains $\partial P/\partial y = R\,\theta$. If the boundary condition $\partial P/\partial y = R\,\theta$ is coupled with $\theta = 0$, one gets $\partial P/\partial y = 0$, meaning that the pressure disturbance is constant along the vertical interface, say $x = 0$. The value of this constant can be chosen arbitrarily, since P appears only through its derivatives in the governing equations. Thus, one can set $P = 0$, i.e. the sidewall boundary condition employed in our paper. In other words, there is no difference between the momentum boundary condition invoked in our paper and that used in Rees and Tyvand (2004). However, it must be pointed out that Rees and Tyvand (2004) couple the momentum boundary condition $\partial P/\partial y = R\theta$ with a temperature boundary condition of vanishing normal heat flux, $\partial\theta/\partial x = 0$, so that their momentum boundary condition cannot be consistently simplified to $P = 0$.

3.1 Normal Modes

According to the usual normal mode decomposition, we may write

$$\begin{aligned} P(x, y, z, t) &= e^{\xi_n t} f_n(y)\, \sin\left(\frac{n\pi x}{s}\right) \cos(az), \\ \theta(x, y, z, t) &= e^{\xi_n t} h_n(y)\, \sin\left(\frac{n\pi x}{s}\right) \cos(az), \end{aligned} \tag{14}$$

where n is a positive integer, ξ_n is a complex exponential coefficient, and a is a real parameter with the meaning of a dimensionless wave number. The real part of ξ_n, $\Re(\xi_n)$, determines the stable (if $\Re(\xi_n) < 0$) or unstable (if $\Re(\xi_n) > 0$) character of the perturbation. The neutral stability condition is the threshold between linear stability and instability, namely $\Re(\xi_n) = 0$. The imaginary part of ξ_n, $\Im(\xi_n)$, is the dimensionless angular frequency of the normal mode.

We substitute Eq. (14) into Eqs. (12) so that we obtain

$$f_n'' - \left(a^2 + \frac{n^2\pi^2}{s^2}\right) f_n - R\, h_n' = 0, \tag{15a}$$

$$h_n'' - \left(a^2 + \xi_n + \frac{n^2\pi^2}{s^2} - R\right) h_n - f_n' = 0, \tag{15b}$$

with the boundary conditions

$$\begin{array}{ll} y = 0: & f_n' = R\, h_n, \quad h_n' = 0, \\ y = 1: & f_n' = 0, \quad h_n = 0. \end{array} \tag{16}$$

In Eqs. (15) and (16), primes denote derivatives with respect to y. Let us define

$$\varphi_n(y) = -f_n'(y) + R\, h_n(y), \tag{17a}$$

$$b_n^2 = a^2 + \frac{n^2\pi^2}{s^2}, \tag{17b}$$

then (15) and (16) can be reformulated as

$$\varphi_n'' - b_n^2 \varphi_n + R\, b_n^2 h_n = 0, \tag{18a}$$

$$h_n'' - \left(b_n^2 + \xi_n\right) h_n + \varphi_n = 0, \tag{18b}$$

with the boundary conditions

$$\begin{array}{ll} y = 0: & \varphi_n = 0, \quad h_n' = 0, \\ y = 1: & \varphi_n = 0, \quad h_n = 0. \end{array} \tag{19}$$

3.2 Exchange of Stabilities

The principle of exchange of stabilities entails that the neutral stability condition is associated with non-oscillatory modes. In fact, as a consequence of Eqs. (18) and (19), we will prove that $\Im(\xi_n) = 0$.

We multiply Eq. (18a) by the complex conjugate of φ_n, denoted as φ_n^*, and we integrate by parts with respect to y in the interval $0 \le y \le 1$, by taking into account Eq. (19),

$$-\int_0^1 |\varphi_n'|^2\, dy - b_n^2 \int_0^1 |\varphi_n|^2\, dy + R\, b_n^2 \int_0^1 \varphi_n^* h_n\, dy = 0. \tag{20}$$

Likewise, we multiply Eq. (18b) by the complex conjugate of h_n and we integrate by parts with respect to y in the interval $0 \le y \le 1$,

$$-\int_0^1 |h_n'|^2\, dy - \left(b_n^2 + \xi_n\right) \int_0^1 |h_n|^2\, dy + \int_0^1 h_n^* \varphi_n\, dy = 0. \tag{21}$$

We now sum the complex conjugate of Eq. (20)) and Eq. (21) multiplied by $-R\, b_n^2$, so that we obtain

$$-\int_0^1 |\varphi_n'|^2\, dy - b_n^2 \int_0^1 |\varphi_n|^2\, dy + R\, b_n^2 \int_0^1 |h_n'|^2\, dy + R\, b_n^2 \left(b_n^2 + \xi_n\right) \int_0^1 |h_n|^2\, dy = 0. \tag{22}$$

Equation (22) is satisfied if both the real part and the imaginary part of its left hand side are zero. In particular, since R and b_n are real, the imaginary part of the left hand side of Eq. (22) is zero if

$$R\, b_n^2\, \Im(\xi_n) \int_0^1 |h_n|^2\, dy = 0. \tag{23}$$

Since an eigenfunction, h_n, cannot be identically zero, the integral in Eq. (23) is nonzero. Therefore, Eq. (23) can be satisfied only with $\Im(\xi_n) = 0$. This proves that the principle of exchange of stabilities holds true, and that the analysis of neutral stability can be carried out for stationary normal modes, without any loss of generality. As a consequence, at neutral stability, Eqs. (18) are replaced by

$$\varphi_n'' - b_n^2 \varphi_n + R\, b_n^2 h_n = 0, \tag{24a}$$

$$h_n'' - b_n^2 h_n + \varphi_n = 0. \tag{24b}$$

4 Analytical Solution

The solution of Eqs. (24) with the boundary conditions, Eq. (19), can be determined by employing the usual method of the characteristic equation. Since the boundary value problem is homogeneous, the solution is to be determined up to an arbitrary scale factor. This scale factor can be fixed, without any loss of generality, so that

$$h_n(0) = 1. \tag{25}$$

Then, we may write

$$\begin{aligned} \varphi_n(y) &= b_n \sqrt{R} \left[A_n\, \sin(\lambda_n y) + \frac{1}{2}\, \cos(\lambda_n y) + \frac{A_n \lambda_n}{\eta_n}\, \sinh(\eta_n y) - \frac{1}{2}\, \cosh(\eta_n y) \right], \\ h_n(y) &= A_n\, \sin(\lambda_n y) + \frac{1}{2}\, \cos(\lambda_n y) - \frac{A_n \lambda_n}{\eta_n}\, \sinh(\eta_n y) + \frac{1}{2}\, \cosh(\eta_n y)\,, \end{aligned} \tag{26}$$

where

$$\begin{aligned} \lambda_n &= \sqrt{b_n \left(\sqrt{R} - b_n \right)}, \\ \eta_n &= \sqrt{b_n \left(\sqrt{R} + b_n \right)}, \\ A_n &= \frac{\eta_n \left(\cosh \eta_n - \cos \lambda_n \right)}{2 \left(\eta_n \sin \lambda_n + \lambda_n \sinh \eta_n \right)}. \end{aligned} \tag{27}$$

Equations (26) and (27) ensure that Eqs. (24), (25) are satisfied, together with the boundary conditions, given by Eq. (19): $\varphi_n(0) = \varphi_n(1) = 0$ and $h_n'(0) = 0$. On the other hand, the last boundary condition, $h_n(1) = 0$, leads to the dispersion relation

$$\frac{\lambda_n \sinh \eta_n \cos \lambda_n + \eta_n \cosh \eta_n \sin \lambda_n}{\eta_n \sin \lambda_n + \lambda_n \sinh \eta_n} = 0. \tag{28}$$

Equations (17b), (27), and (28) allow one to plot the neutral stability curves in the parametric plane (a, R), for any given aspect ratio s.

5 Discussion of the Results

The dispersion relation, Eq. (28), can be displayed in the parametric plane (b_n, R). Obviously, if we do not specify the modal number n and the transverse aspect ratio s, the parameter b_n is nothing but a redefined wave number that can vary continuously over the set of positive real numbers. In this case, for the sake of simplicity, we denote b_n with b and plot Eq. (28) in the plane (b, R). This plot is shown in Fig. 2. There are two disconnected branches, each one displaying a minimum. The lower branch has a minimum for

$$b = 2.326215, \qquad R = 27.09763, \tag{29}$$

while the upper branch has a minimum for

$$b = 5.468656, \qquad R = 132.3633. \tag{30}$$

We note that the lower branch is that describing the transition to instability. When R is below this curve, for a given b, we have in fact linear stability. Then, the pair (b, R) given by Eq. (29) is the critical pair for the onset of instability. We mention that the same critical value of R was found by Ribando and Torrance (1976), and more recently by Wang (1999) on studying the stability of a saturated rectangular porous box with lateral impermeable and adiabatic boundaries, upper horizontal wall maintained at constant temperature, and lower horizontal wall heated by a constant flux.

Due to the lateral confinement, with a given aspect ratio s, the longitudinal wave number a is related to b_n through Eq. (17b), so that we can plot the neutral stability curves with respect to a for prescribed modal numbers n. These plots are displayed in Figs. 3, 4, 5, 6, 7, 8, relative to the aspect ratios $s = 1/2,\ 3/4,\ 1,\ 3/2,\ 2,\ 5/2$. The aspect ratio $s = 1$ (Fig. 5) is for a square channel, while $s < 1$ (Figs. 3, 4) is for a slender rectangular channel, and $s > 1$ (Figs. 6, 7, 8) is for a shallow rectangular channel.

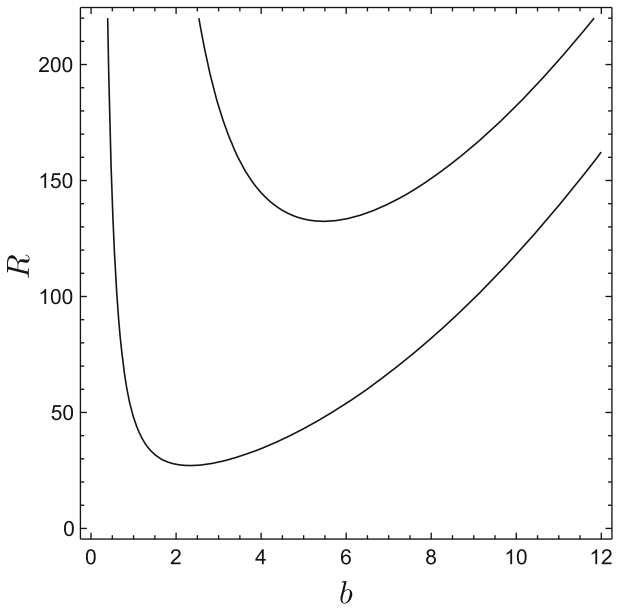

Fig. 2 Neutral stability curves in the plane (b, R)

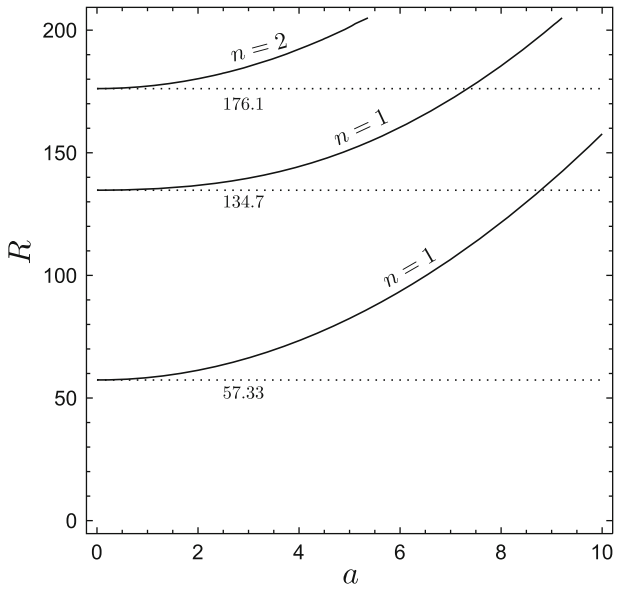

Fig. 3 Neutral stability curves in the plane (a, R) for $s = 1/2$. The *dotted lines* denote the minimum of each branch

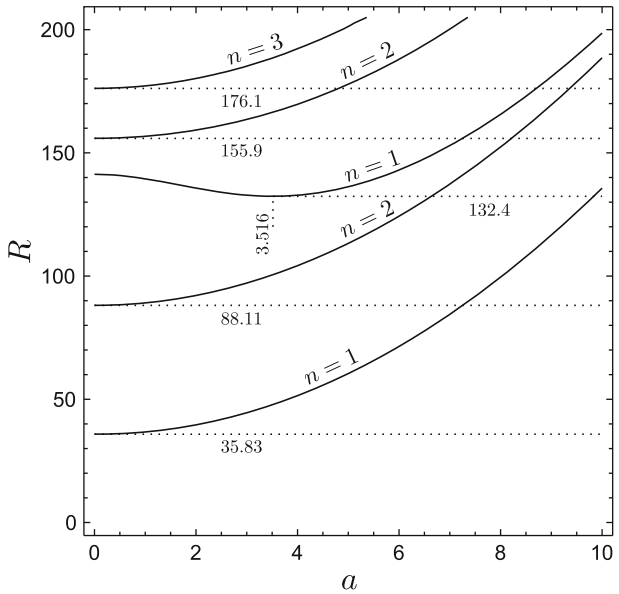

Fig. 4 Neutral stability curves in the plane (a, R) for $s = 3/4$. The *dotted lines* denote the minimum of each branch

Figures 3, 4, 5 show that the most unstable modes are those with $n = 1$ and that the onset of convection takes place for vanishingly small wave numbers, meaning z independent or two-dimensional modes. In particular, for $s = 1/2,\ 3/4,\ 1$, the critical wave number is $a_c = 0$ and the critical values of R are $R_c = 57.33,\ 35.83,\ 29.21$, respectively. This

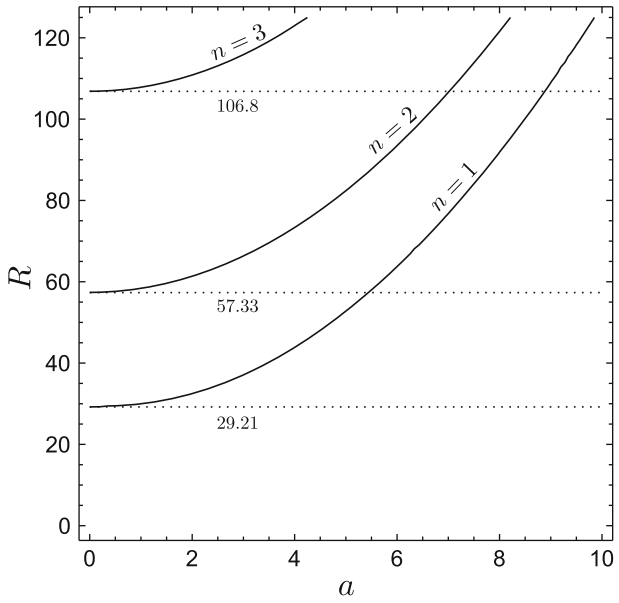

Fig. 5 Neutral stability curves in the plane (a, R) for $s = 1$. The *dotted lines* denote the minimum of each branch

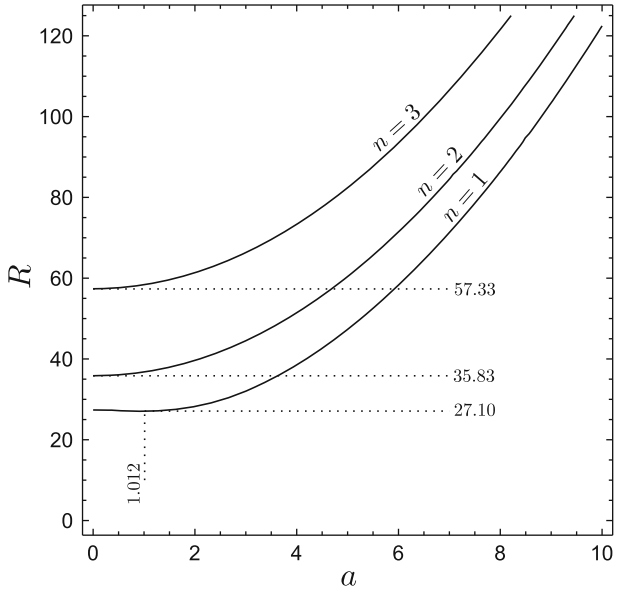

Fig. 6 Neutral stability curves in the plane (a, R) for $s = 3/2$. The *dotted lines* denote the minimum of each branch

behaviour changes slightly in Fig. 6 where, even if the least stable modes are still for $n = 1$, we have a nonvanishing critical wave number $a_c = 1.012$ and a critical Darcy–Rayleigh number $R_c = 27.10$, viz. just the same value of R reported in Eq. (29). We mention that the

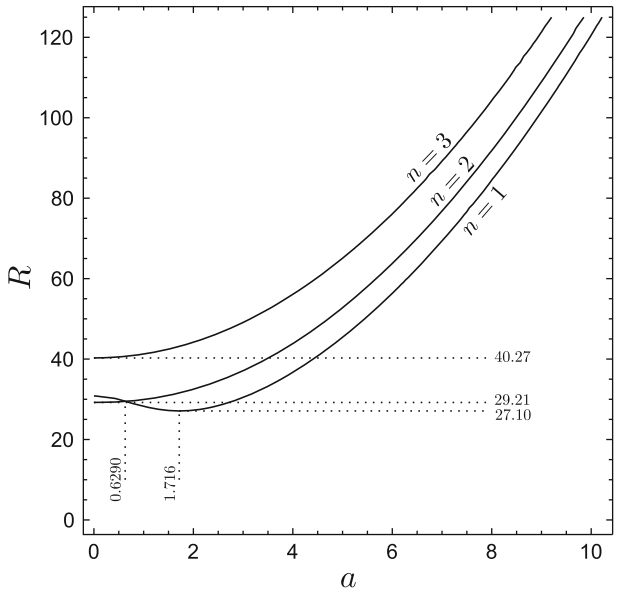

Fig. 7 Neutral stability curves in the plane (a, R) for $s = 2$. The *dotted lines* denote the minimum of each branch and the intersection between different branches

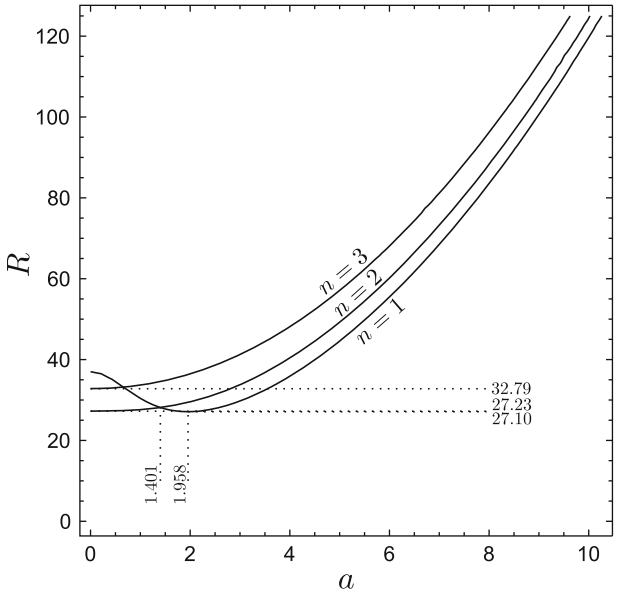

Fig. 8 Neutral stability curves in the plane (a, R) for $s = 5/2$. The *dotted lines* denote the minimum of each branch and the intersection between different branches

value $a_c = 1.012$ arises by taking the value of b from Eq. (30) and by employing Eq. (17b) with $n = 1$ and $s = 3/2$. The transition from a condition with $a_c = 0$ to one with $a_c > 0$ occurs with a value of s intermediate between $s = 1$ (Fig. 5) and $s = 3/2$ (Fig. 5). A precise evaluation of this transition aspect ratio yields

$$s = 1.350517. \tag{31}$$

Below this aspect ratio, the onset of convection is two-dimensional (z-independent), while for higher aspect ratios the selected modes at neutral stability are three-dimensional. Relative to a shallow channel, Figs. 7 and 8 show that the modes with $n = 1$ are not the most unstable over the whole range of a, but only for sufficiently large wave numbers: $a > 0.6290$ and $a > 1.401$ for $s = 2$ and $s = 5/2$, respectively. For smaller wave numbers, the modes with $n = 2$ prevail. Anyway, the absolute minimum of R for neutral stability takes place for $n = 1$ in both cases, and this is for a nonvanishing critical wave number. Another interesting feature displayed by Figs. 5, 6, 7, 8 is that, on increasing the aspect ratio s, the neutral stability curves with $n = 1, 2, 3$ become closer and closer, meaning an easier transition between different modes at slightly supercritical conditions.

6 A Channel with Finite Longitudinal Length

Let us now assume that the longitudinal length is finite, so that the channel has end boundaries $z = 0$ and $z = s/\ell$. In this case, the porous channel should rather be termed a rectangular porous box. The quantity ℓ has the meaning of a width-to-length aspect ratio. With a finite length in the z direction, the axial wave number a cannot be continuous. On the other hand, depending on the type of boundary conditions on P and θ prescribed at $z = 0$ and $z = s/\ell$, we have a discrete sequence of allowed wave numbers $\{a_m;\ m = 1, 2, 3, \ldots\}$.

6.1 Adiabatic and Impermeable end Boundaries

Assuming adiabatic and impermeable end boundaries, both $\partial P/\partial z$ and $\partial\theta/\partial z$ must vanish at $z = 0$ and $z = s/\ell$. Thus, Eq. (14) yields a restriction on the allowed values of a. The wave number can only be given by the sequence of values,

$$a_m = \frac{m\pi\ell}{s}, \qquad m = 0, 1, 2, \ldots, \tag{32}$$

so that the modified wave number b, Eq. (17b), now admits the sequence of values,

$$b^2_{m,n} = \frac{\pi^2}{s^2}\left(m^2\ell^2 + n^2\right), \qquad m = 0, 1, 2, \ldots, \quad n = 1, 2, 3, \ldots. \tag{33}$$

Thus, the possible normal modes of neutral stability are now labelled by the pair (m, n). The modes with $m = 0$ are z-independent and, hence, they are two-dimensional. Equation (33) proves that these modes are also independent of ℓ. Figure 9 shows the trend of R versus s for the $m = 0$ modes, revealing the most unstable n-modes for the different ranges of s. The ordering of the $(0, n)$-modes is simple and relies just on Eq. (33), as the dispersion relation Eq. (28) depends on b and R. Therefore, as s increases, the most unstable $(0, n)$-mode is found in increasing order of n. The task is more complicated when one considers all possible (m, n)-modes. In this case, the aim is determining the most unstable mode for each assigned (ℓ, s). This means tiling the parametric (ℓ, s)-plane with the specification of the selected (m, n)-mode in each subdomain. This kind of analysis was initiated in the literature with the study reported by Beck (1972). We note that, for every assigned ℓ, there is a sequence of least stable (m, n)-modes displayed when s gradually increases. The ordering of the (m, n)-modes in this sequence depends on ℓ, and it can be determined on account of Eq. (33). It is just a matter of setting the values of $m^2\ell^2 + n^2$ in increasing order.

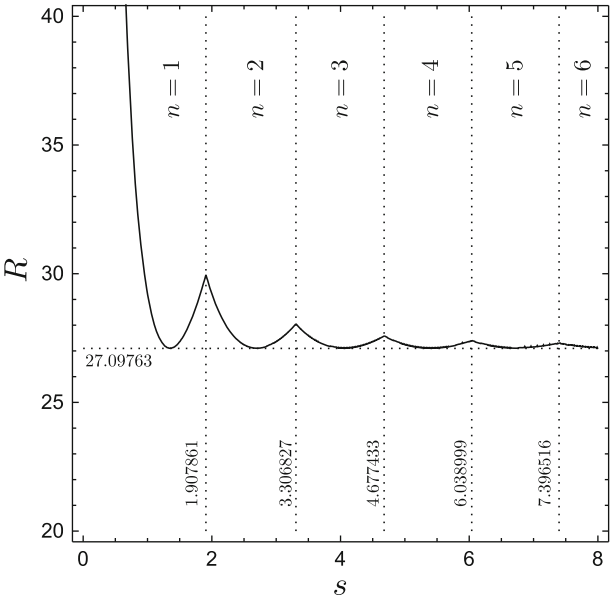

Fig. 9 Finite longitudinal length: adiabatic and impermeable end conditions. Neutral stability curve $R(s)$ for the $m = 0$ modes

The mode-selection diagram associated with Eqs. (28), (32), and (33) is given in Fig. 10. We mention that vanishingly small values of ℓ describe an infinitely long channel, and hence the conditions assumed in the preceding sections. On the other hand, increasing values of ℓ describe a shorter and shorter channel. This limit is relatively simple to deal with, as it implies a continuous change of the longitudinal wave number. In spite of that, the condition of a very long (but finite) channel is quite complicated to describe, as we may have different but almost equivalent (m, n)-modes arising as the most unstable with extremely small changes of either ℓ or s. A similar complexity is found when ℓ is fixed and s is very large. Figure 10, although relative to a limited domain in the (ℓ, s)-plane, confirms this finding.

Figure 10 suggests that with s smaller than the threshold value given by Eq. (31) the preferred mode is (0, 1), meaning $m = 0$ and $n = 1$, for every $\ell > 0$. The mode-selection diagram, Fig. 10, shows that the threshold value of s increases with ℓ and that, for $\ell > \sqrt{3}$, it becomes constant: $s = 1.907861$. The system displays a preference for two dimensional, z-independent, modes as long as the shape of the transverse cross-section is not too shallow. When the longitudinal length is sufficiently small ($\ell > \sqrt{3}$) the (0, 1)-mode slides into the (0, 2)-mode which is also two-dimensional, while s increases above 1.907861. On the other hand, for longer channels ($\ell < \sqrt{3}$), the transition is from the (0, 1)-mode to the three-dimensional (1, 1)-mode.

6.2 Conducting and Permeable End Boundaries

If the boundaries $z = 0$ and $z = s/\ell$ are conducting and permeable, the temperature perturbation and the pressure perturbation must vanish. In other words, the boundary conditions for P and θ to be prescribed at $z = 0$ and $z = s/\ell$ are just the same as those assigned at $x = 0$ and $x = s$. The latter boundary conditions are given by Eq. (13). This means that Eq. (14) for stationary modes needs to be replaced by

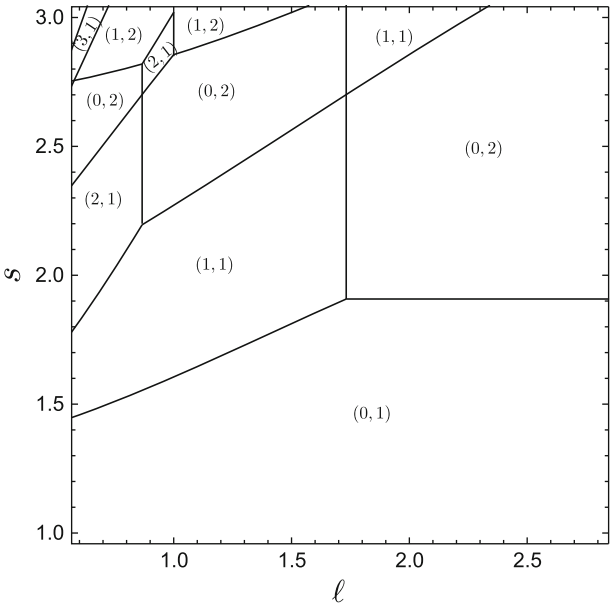

Fig. 10 Finite longitudinal length: adiabatic and impermeable end conditions. Map of selected (m, n)-modes at onset of instability for different ranges of ℓ and s

$$
\begin{aligned}
P(x, y, z, t) &= e^{\xi_n t} f_n(y) \sin\left(\frac{n\pi x}{s}\right) \sin(az), \\
\theta(x, y, z, t) &= e^{\xi_n t} h_n(y) \sin\left(\frac{n\pi x}{s}\right) \sin(az).
\end{aligned}
\tag{34}
$$

This adjustment does not have any influence in the formulation of Eq. (15), in the proof of the principle of exchange of stabilities, and in the analytical solution discussed in Sect. 4.

The wave number selection, from Eq. (34), requires that both P and θ vanish at $z = s/\ell$. We can immediately conclude that this selection of wave numbers, a, is just the same as that defined by Eqs. (32) and (33) except for the exclusion of the modes with $m = 0$. Actually, setting $a = a_0 = 0$ now would mean, from Eq. (34), identically vanishing perturbations P and θ. As a consequence, no z-independent normal modes are allowed in this case. The lowest order m-modes are with $m = 1$ and their neutral stability curves are depicted in Fig. 11. We observe that the dependence on z implies a dependence on the aspect ratio ℓ which is quite evident in Fig. 11 on comparing $\ell = 0.01,\ 1,\ 1.5$. We recall that $\ell = 0.01$ means a very long channel (with respect to transverse width). In fact, we recognise a close similarity between the solid curve ($\ell = 0.01$) in Fig. 11 and the neutral stability curve in Fig. 9 for the end conditions defined in Sect. 6.1. This feature is to be expected, as the behaviour for a very long channel depends weakly on the end conditions.

Figure 12 is the mode-selection diagram for conducting and permeable end conditions. We see that, for sufficiently small values of s, the three-dimensional mode (1,1) is selected as the most unstable.

6.3 Hybrid End Conditions

A pair of end conditions intermediate between those defined in Sects. 6.1 and 6.2 is such that one end is assumed adiabatic and impermeable, while the other is considered conducting and

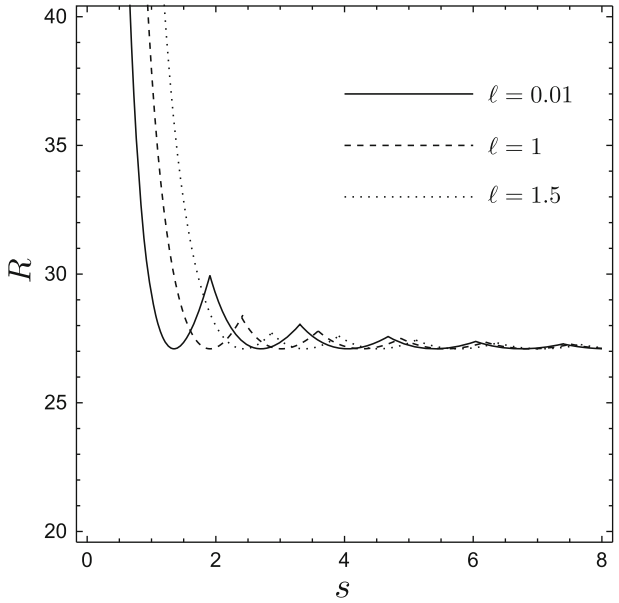

Fig. 11 Finite longitudinal length: conducting and permeable end conditions. Neutral stability curves $R(s)$ for the $m = 1$ modes with different values of ℓ

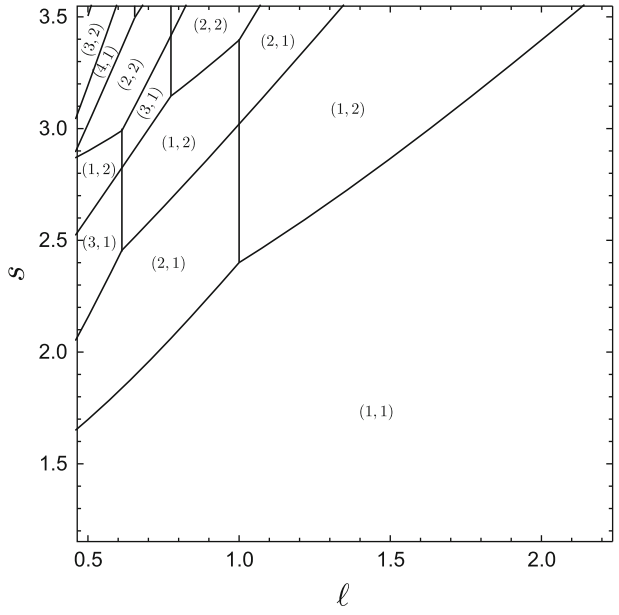

Fig. 12 Finite longitudinal length: conducting and permeable end conditions. Map of selected (m, n)-modes at onset of instability for different ranges of ℓ and s

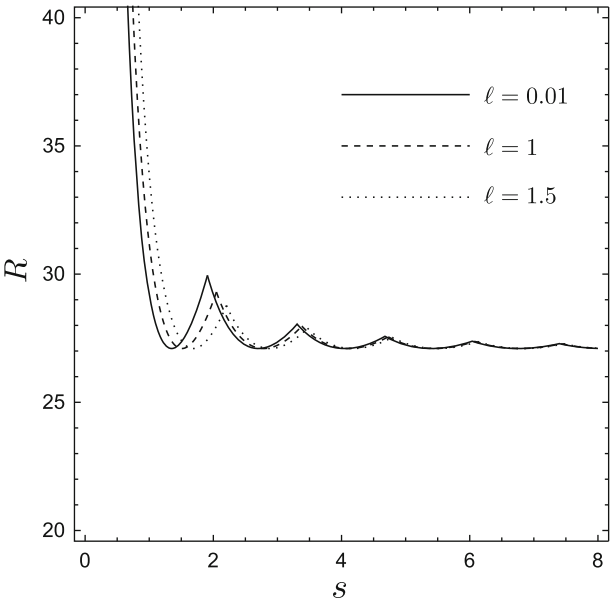

Fig. 13 Finite longitudinal length: hybrid end conditions, Eq. (35). Neutral stability curves $R(s)$ for the $m = 0$ modes with different values of ℓ

permeable. It is not restrictive to take the former as the boundary $z = 0$, while the latter is the boundary $z = s/\ell$, namely

$$\begin{aligned} &z = 0; \quad 0 < x < s; \quad 0 < y < 1: \qquad \frac{\partial P}{\partial z} = 0, \quad \frac{\partial \theta}{\partial z} = 0, \\ &z = s/\ell; \quad 0 < x < s; \quad 0 < y < 1: \qquad P = 0, \quad \theta = 0. \end{aligned} \tag{35}$$

As a consequence, Eq. (14) still holds. However, the selected wave numbers are not those expressed by Eqs. (32) and (33). In fact, these equations are to be replaced by

$$a_m = \left(m + \frac{1}{2}\right)\frac{\pi\ell}{s}, \qquad m = 0, 1, 2, \ \ldots \ , \tag{36}$$

$$b_{m,n}^2 = \frac{\pi^2}{s^2}\left[\left(m + \frac{1}{2}\right)^2 \ell^2 + n^2\right], \qquad m = 0, 1, 2, \ \ldots \ , \quad n = 1, 2, 3, \ \ldots \ . \tag{37}$$

Comparisons of Figs. 13 and 14 both with Figs. 9 and 10, and with Figs. 11 and 12 suggest that the hybrid end conditions lead to a behaviour intermediate between those reported in Sects. 6.1 and 6.2. We point out that the $m = 0$ modes are three-dimensional, differently from the $m = 0$ modes considered in Sect. 6.1. Hence, Fig. 13 displays an ℓ-dependence, although markedly weaker than in Fig. 11. Furthermore, Figs. 10 and 14 reveal strong analogies. In particular, the three-dimensionality of the modes $m = 0$ is the reason why, in Fig. 14, the curve separating the domain of the mode (0, 1) from that of the mode (0,2) is not a straight horizontal line as in Fig. 10.

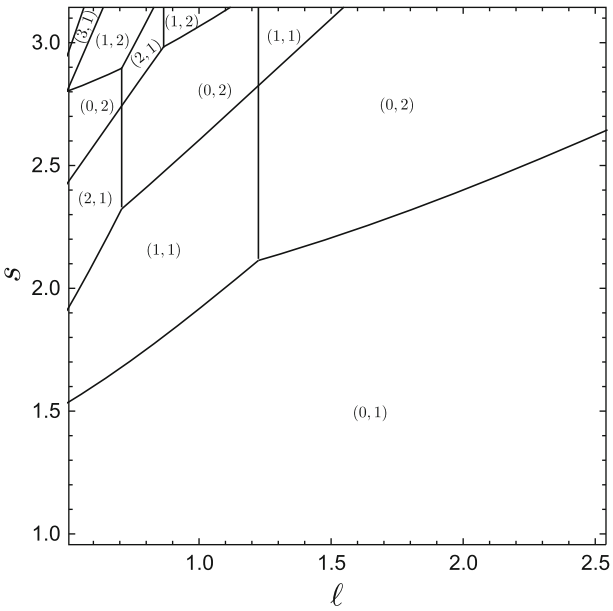

Fig. 14 Finite longitudinal length: hybrid end conditions, Eq. (35). Map of selected (m, n)-modes at onset of instability for different ranges of ℓ and s

7 Conclusions

We have studied the stability versus small-amplitude disturbances of the steady motionless state in a horizontal rectangular channel containing a fluid-saturated porous material. Heating from below has been modelled on a uniform flux, while cooling from above is due to an isothermal upper boundary. A lateral confinement has been described by assuming thermal and mechanical contact with a saturated porous reservoir in a steady state with vertical thermal stratification.

Darcy's law and the Oberbeck–Boussinesq approximation have been adopted to model the buoyant flow. The dimensionless parameters governing the onset of the instability are the Darcy–Rayleigh number, R, and the width-to-height aspect ratio, s. An analytical solution of the disturbance equations has been found for the normal modes. These modes are labelled by the natural number, n, such that $n-1$ yields the number of nodes of the sinusoidal temperature distribution in the transverse horizontal direction, namely along the x axis.

A study of the neutral stability curves has been carried out for different aspect ratios ranging from $s = 1/2$ to $s = 5/2$. The main feature revealed by this study is that the modes with $n = 1$ are preferred at onset of convection. However, the critical condition, defined as the absolute minimum of R leading to instability, may be displayed either with two-dimensional instability patterns or three-dimensional patterns. The former are rolls invariant along the longitudinal z direction. The three-dimensional patterns are preferred at the onset of instability when the aspect ratio is sufficiently large, viz. exceeding the threshold value $s = 1.350517$. Under these conditions, the absolute minimum of R leading to instability is the critical value $R = 27.09763$.

The effect of a finite longitudinal length along the horizontal z axis has been investigated, so that a secondary aspect ratio, ℓ, has been defined. With this respect, specific assumptions

about the end planes, $z =$ constant, bounding longitudinally the channel have been made. We considered three different cases: adiabatic and impermeable end conditions, conducting and permeable end conditions, hybrid end conditions. The third case displays a neutral stability behaviour intermediate between the first case and the second case, and is defined by assuming adiabatic and impermeable conditions at $z = 0$, and conducting and permeable conditions at $z = s/\ell$. For the three different models of end conditions at $z = 0$ and $z = s/\ell$, diagrams have been drawn showing the preferred modes selected at the onset of instability. Only with adiabatic and impermeable end conditions two-dimensional modes can be selected, although these modes may not be the most unstable for every pair of aspect ratios (s, ℓ).

Acknowledgments This study was financially supported by Italian government with MIUR–PRIN program Grant 2009KSSKL3.

References

Barletta, A.: Thermal instabilities in a fluid saturated porous medium. In: Öchsner, A., Murch, G.E. (eds.) Heat Transfer in Multi-phase Materials, pp. 381–414. Springer, New York (2011)

Barletta, A., Storesletten, L.: A three-dimensional study of the onset of convection in a horizontal, rectangular porous channel heated from below. Int. J. Therm. Sci. **55**, 1–15 (2012)

Beck, J.L.: Convection in a box of porous material saturated with fluid. Phys. Fluids **15**, 1377–1383 (1972)

Horton, C.W., Rogers, F.T.: Convection currents in a porous medium. J. Appl. Phys. **16**, 367–370 (1945)

Lapwood, E.R.: Convection of a fluid in a porous medium. Proc. Camb. Philos. Soc. **44**, 508–521 (1948)

Nield, D.A., Bejan, A.: Convection in Porous Media, 3rd edn. Springer, New York (2006)

Nilsen, T., Storesletten, L.: An analytical study on natural convection in isotropic and anisotropic porous channels. ASME J. Heat Transf. **112**, 396–401 (1990)

Nygård, H.S., Tyvand, P.A.: Onset of convection in a porous box with partly conducting and partly penetrative sidewalls. Transp. Porous Media **84**, 55–73 (2010)

Nygård, H.S., Tyvand, P.A.: Onset of thermal convection in a vertical porous cylinder with a partly conducting and partly penetrative cylinder wall. Transp. Porous Media **86**, 229–241 (2011)

Rees, D.A.S.: The stability of Darcy–Bénard convection. In: Vafai, K., Hadim, H.A. (eds.) Handbook of Porous Media, Chap. 12, pp. 521–558. CRC Press, New York (2000)

Rees, D.A.S., Tyvand, P.A.: Oscillatory convection in a two-dimensional porous box with asymmetric lateral boundary conditions. Phys. Fluids **16**, 3706–3714 (2004)

Ribando, R.J., Torrance, K.E.: Natural convection in a porous medium: effects of confinement, variable permeability, and thermal boundary conditions. ASME J. Heat Transf. **98**, 42–48 (1976)

Straughan, B.: Stability and Wave Motion in Porous Media. Springer, New York (2008)

Sutton, F.M.: Onset of convection in a porous channel with net through flow. Phys. Fluids **13**, 1931–1934 (1970)

Tyvand, P.A.: Onset of Rayleigh–Bénard convection in porous bodies. In: Ingham, D.B., Pop, I. (eds.) Transport Phenomena in Porous Media II, Chap. 4, pp. 82–112. Pergamon, New York (2002)

Wang, C.Y.: Onset of convection in a fluid-saturated rectangular box, bottom heated by constant flux. Phys. Fluids **11**, 1673–1675 (1999)